Berry phase in superconducting multiterminal quantum dots

Benoît Douçot,[1,*] Romain Danneau,[2] Kang Yang,[1,3] Jean-Guy Caputo,[4] and Régis Mélin[5]
[1]*Laboratoire de Physique Théorique et Hautes Energies, Sorbonne Université and CNRS UMR 7589, 4 place Jussieu, 75252 Paris Cedex 05, France*
[2]*Institute of Nanotechnology, Karlsruhe Institute of Technology, D-76021 Karlsruhe, Germany*
[3]*Laboratoire de Physique des Solides, CNRS UMR 8502, Université Paris–Sud, Université Paris–Saclay, F-91405 Orsay Cedex, France*
[4]*Laboratoire de Mathématiques, INSA de Rouen, Avenue de l'Université, F-76801 Saint-Etienne du Rouvray, France*
[5]*Université Grenoble–Alpes, CNRS, Grenoble INP, Institut NEEL, 38000 Grenoble, France*

(Received 5 April 2019; revised manuscript received 29 November 2019; published 13 January 2020)

We report on a study of the nontrivial Berry phase in superconducting multiterminal quantum dots biased at commensurate voltages. Starting with the time-periodic Bogoliubov–de Gennes equations, we obtain a tight-binding model in Floquet space, and we solve these equations in the semiclassical limit. We observe that the parameter space defined by the contact transparencies and quartet phase splits into two components with a nontrivial Berry phase. We use the Bohr-Sommerfeld quantization to calculate the Berry phase. We find that if the quantum dot level sits at zero energy, then the Berry phase takes the values $\varphi_B = 0$ or $\varphi_B = \pi$. We demonstrate that this nontrivial Berry phase can be observed by tunneling spectroscopy in the Floquet spectra. Consequently, the Floquet-Wannier-Stark ladder spectra of superconducting multiterminal quantum dots are shifted by half-a-period if $\varphi_B = \pi$. Our numerical calculations based on the Keldysh Green's functions show that this Berry phase spectral shift can be observed from the quantum dot tunneling density of states.

DOI: 10.1103/PhysRevB.101.035411

I. INTRODUCTION

The geometric phase is a general concept common to both classical and quantum physics [1]. In a quantum system, the wave function can accumulate a geometric phase, also called the Berry phase, following cyclic adiabatic evolution around the phase space origin [2–6]. Over the years, the Berry phase has been studied extensively both theoretically and experimentally [5,6] as it can provide deep insight into fundamental problems in qubits [7–10], topological insulators [11], skyrmions [12], single and bilayer graphene [13–16], molecular physics [17], and Bose-Einstein condensates [18,19], to cite but a few.

Recently, superconducting multiterminal devices have triggered broad interest due to many exotic phenomena uncovered in these systems, such as the emergence of Majorana fermions [20–22], topological states associated with zero-energy Andreev bound states (ABSs) and Weyl singularities [23–27], or new correlations among pairs of Cooper pairs, so-called quartets [28–32]. As a new kind of elementary process, the quartets appear when the leads are driven by commensurate voltages in a three-terminal geometry (see Fig. 1), and they occur as the differential resistance features [30,32] theoretically predicted in Ref. [28]. Moreover, in the case of superconducting quantum dots (QDs), we have recently demonstrated that nontrivial ABS time-periodic dynamics yields sharp resonances in the Floquet energy spectrum [33,34]. Interestingly, these Floquet-Wannier-Stark (FWS) ladders in the presence of quartets exhibit Landau-Zener-Stückelberg interference patterns [34–36].

In this article, we present analytical calculations of the FWS ladder spectrum in superconducting multiterminal QDs, in the limit of small dc voltage bias. In this limit, we can use the semiclassical approximation, which shows that the FWS spectrum is controlled by the value of a Berry phase. We find that if the quantum dot level sits at zero energy, a nontrivial Berry phase $\varphi_B = \pi$ can develop under commensurate voltage biasing on the quartet line. We obtain the Bohr-Sommerfeld quantization condition by matching the semiclassical wave functions between the different pieces of the classical trajectories in phase space. We use the quartet phase and superconducting contact transparencies as a parameter space that is divided into two regions with $\varphi_B = 0$ and $\varphi_B = \pi$, separated by a hypersurface on which the gap closes between the dynamically generated Andreev bands. Finally, we confirm our analytical theory by obtaining evidence for the characteristic half-a-period spectral shift in the FWS ladder spectrum for $\varphi_B = \pi$ from a numerical calculation of the quantum dot tunnel density of states.

This paper is organized as follows. In Sec. II, we introduce the Hamiltonian used as a model of multiterminal superconducting quantum dots. We develop a tight-binding model in Floquet space for these systems in Sec. III. The adiabatic limit, relevant for small dc voltage biases, is presented in Sec. IV, in which the FWS spectrum is shown to depend on a Berry phase. This phase is controlled by a winding number, whose phase diagram in parameter space is shown. The tunneling spectra together with the numerical results on the shifted FWS ladder induced by the nontrivial Berry phase are presented in Sec. V. A summary and perspectives are provided in Sec. VI.

*doucot@lpthe.jussieu.fr

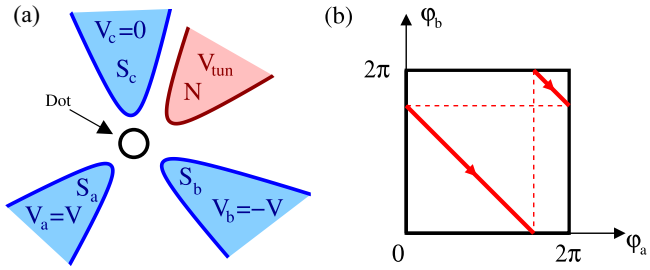

FIG. 1. (a) A superconducting three-terminal QD biased on the quartet line at voltages $V_{a,b} = \pm V$ and $V_c = 0$, with in addition a tunnel-contacted normal lead to probe the quantum dot density of states. (b) The values of $(\varphi_a(t), \varphi_b(t))$ during one period of Josephson oscillations. Commensurate bias voltage implies that (φ_a, φ_b) encloses a cycle on a two-dimensional torus.

The Appendix gives a detailed presentation of semiclassical calculations, aimed at evaluating the first nonanalytic corrections in Δ/V, which arise from Landau-Zener-Stückelberg transitions between the two FWS ladders originating from the two ABS bands.

II. HAMILTONIAN

We consider in this paper a quantum dot coupled to N superconducting leads, which are biased at commensurate dc voltages V_i $(1 \leqslant i \leqslant N)$. We write $V_i = s_i V$, where s_i is an integer (see Fig. 1). For example, in the so-called quartet configuration we have $N = 3$ and $s_i = 0, \pm 1$.

The Hamiltonian of the superconducting-quantum dot takes the following form:

$$H(t) = H_0 + H_J(t), \tag{1}$$

where H_0 is the BCS Hamiltonian for the superconducting leads, and $H_J(t)$ describes the tunneling processes between these reservoirs and the quantum dot. Specifically,

$$H_0 = \sum_{j=1}^{N} \sum_{\sigma} \int \frac{d^D\mathbf{k}}{(2\pi)^D} (\epsilon(j,\mathbf{k}) c_\sigma^\dagger(j,\mathbf{k}) c_\sigma(j,\mathbf{k}) + \Delta_j c_\uparrow^\dagger(j,\mathbf{k}) c_\downarrow^\dagger(j,-\mathbf{k}) + \Delta_j^* c_\downarrow(j,-\mathbf{k}) c_\uparrow(j,\mathbf{k})), \tag{2}$$

$$H_J = \sum_{j=1}^{N} J_j \sum_{\sigma} \int \frac{d^D\mathbf{k}}{(2\pi)^D} (e^{-is_j\omega_0 t} c_\sigma^\dagger(j,\mathbf{k}) d_\sigma + e^{is_j\omega_0 t} d_\sigma^\dagger c_\sigma(j,\mathbf{k})). \tag{3}$$

Here $c_\sigma^\dagger(j,\mathbf{k})$ and $c_\sigma(j,\mathbf{k})$ are creation and annihilation operators for an electron on reservoir j with momentum $\mathbf{k}$ and spin σ along the quantization axis. The corresponding operators on the dot are denoted by $d_\sigma^\dagger$ and d_σ. The dimension D of the reservoirs is denoted by D (with $D = 3$ in all numerical calculations). The basic frequency ω_0 is associated with single electron tunneling processes, and it is equal to $\omega_0 = eV/\hbar$. We have $\omega_0 = \omega_J/2$, where ω_J is the Josephson frequency associated with V. For simplicity, we assume that the superconducting gaps in all reservoirs take the same value Δ, and we use the notation $\Delta_j = \Delta e^{i\varphi_j}$.

III. FLOQUET QUASIPARTICLE OPERATORS

A. Reduction to a 1D chain

After eliminating the superconducting leads, the Floquet theory of the time-periodic Bogoliubov–de Gennes equations produces an effective one-dimensional (1D) tight-binding model for the two-component Nambu spinors Ψ_m describing the part of the wave function located on the dot. Here, we describe the corresponding demonstration of the 1D tight-binding model.

The Hamiltonian given by Eqs. (1)–(3) is quadratic in the basic fermion operators. Then, the many-body problem reduces to the simpler time-dependent Bogoliubov–de Gennes equations

$$i\frac{d}{dt}\Gamma^\dagger(t) = [H(t), \Gamma^\dagger(t)], \tag{4}$$

where $\Gamma^\dagger(t)$ denotes a quasiparticle creation operator. Because the Hamiltonian is periodic in time with period $T = 2\pi/\omega_0$, the Floquet theorem leads to

$$\Gamma^\dagger(t+T) = e^{-iET/\hbar}\Gamma^\dagger(t). \tag{5}$$

Taking the Hermitian conjugate of Eq. (4) leads to another Floquet solution $\Gamma(t)$, with E changed into its opposite.

The Fourier series of $\Gamma_\sigma^\dagger(t)$ is the following:

$$\Gamma_\sigma^\dagger(t) = e^{-iEt/\hbar} \sum_{m\in\mathbb{Z}} e^{-im\omega_0 t} \Bigg(u_m d_\sigma^\dagger + \sigma v_m d_{-\sigma} + \sum_{i=1}^{N} \int \frac{d^D\mathbf{k}}{(2\pi)^D} [u_m(i,\mathbf{k}) c_\sigma^\dagger(i,\mathbf{k}) + \sigma v_m(i,\mathbf{k}) c_{-\sigma}(i,\mathbf{k})] \Bigg), \tag{6}$$

where E is the Floquet quasienergy. Substituting into Eq. (4) leads to

$$(E + m\omega_0 - \epsilon(i,\mathbf{k}) + i\eta) u_m(i,\mathbf{k}) = \Delta_i v_m(i,\mathbf{k}) + J_i u_{m-s_i}, \tag{7}$$

$$(E + m\omega_0 + \epsilon(i,\mathbf{k}) + i\eta) v_m(i,\mathbf{k}) = \Delta_i^* u_m(i,\mathbf{k}) - J_i v_{m+s_i}, \tag{8}$$

and

$$(E + m\omega_0 + i\eta) u_m = \sum_{i=1}^{N} J_i \int \frac{d^D\mathbf{k}}{(2\pi)^D} u_{m+s_i}(i,\mathbf{k}), \tag{9}$$

$$(E + m\omega_0 + i\eta) v_m = -\sum_{i=1}^{N} J_i \int \frac{d^D\mathbf{k}'}{(2\pi)^D} v_{m-s_i}(i,\mathbf{k}). \tag{10}$$

Here, we have introduced a small positive imaginary part η to the quasienergies. Eliminating the amplitudes in the reservoirs using Eqs. (7) and (8), and substituting into Eqs. (9) and (10),

leads to

$$(E + m\omega_0 + i\eta)u_m - \sum_{i=1}^{N} J_i^2\, U_m^{(i)} = 0, \tag{11}$$

$$(E + m\omega_0 + i\eta)v_m - \sum_{i=1}^{N} J_i^2\, V_m^{(i)} = 0, \tag{12}$$

where

$$U_m^{(i)} = g_{11}^{(i)}(E + (m + s_i)\omega_0)u_m - g_{12}^{(i)}(E + (m + s_i)\omega_0)v_{m+2s_i}, \tag{13}$$

$$V_m^{(i)} = -g_{21}^{(i)}(E + (m - s_i)\omega_0)u_{m-2s_i} + g_{22}^{(i)}(E + (m - s_i)\omega_0)v_m. \tag{14}$$

Later, we will make extensive use of the linear operator acting on the collection of amplitudes u_m, v_m, which appears on the left-hand side of Eqs. (11) and (12). This operator will be denoted by $\mathcal{L}(E)$. We have shown in a previous work [34] that all single-particle creation and annihilation operators can be expressed in terms of the resolvent operator $\mathcal{R}(E) = \mathcal{L}(E)^{-1}$. The function $g_{ab}^{(i)}(\omega)$ is the Fourier transform of the retarded Green's function $g_{\rm ret}^{(i)}(t)$ of the isolated reservoir i on the tunneling site connected to the dot, defined as

$$g_{\rm ret}^{(i)}(t) = -i\begin{pmatrix} \{\Psi_{i,\sigma}(t), \Psi_{i,\sigma}^\dagger(0)\} & \sigma\{\Psi_{i,\sigma}(t), \Psi_{i,-\sigma}(0)\} \\ \sigma\{\Psi_{i,-\sigma}^\dagger(t), \Psi_{i,\sigma}^\dagger(0)\} & \{\Psi_{i,-\sigma}^\dagger(t), \Psi_{i,-\sigma}(0)\} \end{pmatrix}$$

for $t > 0$ and $g_{\rm ret}^{(i)}(t) = 0$ for $t < 0$. Here $\Psi_{i\sigma} = \int \frac{d^D\mathbf{k}'}{(2\pi)^D} c_\sigma(i, \mathbf{k}')$. Explicitly, assuming that $\mathrm{Im}\omega > 0$, we have

$$g^{(i)}(\omega) = \int \frac{d^D\mathbf{k}'}{(2\pi)^D \mathcal{D}(\omega, i, \mathbf{k}')} \begin{pmatrix} \omega + \epsilon(i, \mathbf{k}') & \Delta_i \\ \Delta_i^* & \omega - \epsilon(i, \mathbf{k}') \end{pmatrix},$$

where $\mathcal{D}(\omega, i, \mathbf{k}') = \omega^2 - \epsilon(i, \mathbf{k}')^2 - |\Delta_i|^2$.

Let us introduce the family of two-component spinors $\Psi_m = (u_m, v_m)^T$, labeled by m. We focus on the case of three reservoirs ($N = 3$), with dc bias voltages in the quartet configuration: $s_a = -1$, $s_b = 1$, and $s_c = 0$. In this case, the homogeneous Eqs. (11) and (12) take the form

$$M_0(m)\Psi_m - M_+(m + 1)\Psi_{m+2} - M_-(m - 1)\Psi_{m-2} = 0. \tag{15}$$

The off-diagonal terms in m are second-order Andreev reflection processes between the dot and the reservoirs, which explains why m is coupled to $m \pm 2$. The expanded forms of the matrices $M_0(m)$ and $M_\pm(m)$ are presented in the following subsection.

B. Explicit forms of $M_0(m)$ and $M_\pm(m)$

Now, we provide the expression of the matrices M_0 and $M_\pm$ [see Eq. (15)]. To simplify the discussion, we assume a constant density of states ρ_0 in the normal state. We take the Fermi energy at $\epsilon_F = 0$, and we assume an infinite bandwidth, which implies exact particle-hole symmetry in the leads. This suggests to introduce the integral

$$I(E) = \rho_0 \int_{-\infty}^{\infty} \frac{d\epsilon}{E^2 - |\Delta|^2 - \epsilon^2}. \tag{16}$$

Here, we are interested in the retarded Green's function, and an infinitesimal positive imaginary part is added to energy E. Then, Eq. (16) takes the form

$$I(E) = \frac{-\pi\rho_0}{\sqrt{|\Delta|^2 - E^2}}, \quad E^2 < |\Delta|^2, \tag{17}$$

$$I(E) = \frac{-i\pi\rho_0}{\sqrt{E^2 - |\Delta|^2}}\,\mathrm{sgn}(E), \quad E^2 > |\Delta|^2. \tag{18}$$

The retarded Green's function is then given by

$$g(\omega) = I(\omega)\begin{pmatrix} \omega & \Delta \\ \Delta^* & \omega \end{pmatrix}.$$

Let us now give explicit expressions for the $M_0(m)$ and $M_\pm(m)$ matrices introduced in Eq. (15). The matrices depend also on the energy E. We introduce the variable $\xi = m\omega_0$, where $\omega_0 = eV/\hbar$. The density of states in reservoir j is denoted by $\rho_{0,j}$. It is also convenient to define $\Gamma_j = \pi\rho_{0,j}J_j^2$. We assume $\Delta_j = \Delta e^{i\varphi_j}$. Global gauge invariance allows us to set $\varphi_c = 0$. In the case $|E + \xi| < \Delta$, we have

$$M_0(m) = \begin{pmatrix} (E+\xi)\left(1 + \frac{\sum_j \Gamma_j}{\sqrt{\Delta^2 - (E+\xi)^2}}\right) & -\frac{\Gamma_c\Delta}{\sqrt{\Delta^2-(E+\xi)^2}} \\ -\frac{\Gamma_c\Delta}{\sqrt{\Delta^2-(E+\xi)^2}} & (E+\xi)\left(1 + \frac{\sum_j \Gamma_j}{\sqrt{\Delta^2-(E+\xi)^2}}\right) \end{pmatrix}, \tag{19}$$

$$M_+(m) = \begin{pmatrix} 0 & \frac{\Gamma_b\Delta e^{i\varphi_b}}{\sqrt{\Delta^2-(E+\xi)^2}} \\ \frac{\Gamma_a\Delta e^{-i\varphi_a}}{\sqrt{\Delta^2-(E+\xi)^2}} & 0 \end{pmatrix} \quad \text{and} \quad M_-(m) = \begin{pmatrix} 0 & \frac{\Gamma_a\Delta e^{i\varphi_a}}{\sqrt{\Delta^2-(E+\xi)^2}} \\ \frac{\Gamma_b\Delta e^{-i\varphi_b}}{\sqrt{\Delta^2-(E+\xi)^2}} & 0 \end{pmatrix}. \tag{20}$$

In the case $|E + \xi| > \Delta$, these expressions become

$$M_0(m) = \begin{pmatrix} (E+\xi)\left(1 + i\frac{\sum_j \Gamma_j}{\sqrt{(E+\xi)^2-\Delta^2}}\right) & -\frac{i\Gamma_c\Delta}{\sqrt{(E+\xi)^2-\Delta^2}} \\ -\frac{i\Gamma_c\Delta}{\sqrt{(E+\xi)^2-\Delta^2}} & (E+\xi)\left(1 + i\frac{\sum_j \Gamma_j}{\sqrt{(E+\xi)^2-\Delta^2}}\right) \end{pmatrix}, \tag{21}$$

$$M_+(m) = \begin{pmatrix} 0 & \frac{i\Gamma_b\Delta e^{i\varphi_b}}{\sqrt{(E+\xi)^2-\Delta^2}} \\ \frac{i\Gamma_a\Delta e^{-i\varphi_a}}{\sqrt{(E+\xi)^2-\Delta^2}} & 0 \end{pmatrix} \quad \text{and} \quad M_-(m) = \begin{pmatrix} 0 & \frac{i\Gamma_a\Delta e^{i\varphi_a}}{\sqrt{(E+\xi)^2-\Delta^2}} \\ \frac{i\Gamma_b\Delta e^{-i\varphi_b}}{\sqrt{(E+\xi)^2-\Delta^2}} & 0 \end{pmatrix}. \tag{22}$$

From these matrices, we build the 2×2 matrix $L_0(\xi, k)$. This matrix will be used to obtain the classical trajectories according to $\det L_0(\xi, k) = 0$ in our semiclassical treatment in the forthcoming section. We have

$$L_0(\xi,k) = \begin{pmatrix} (E+\xi)\left(1+\frac{\sum_j \Gamma_j}{\sqrt{\Delta^2-(E+\xi)^2}}\right) & -\frac{(\Gamma_a e^{i(\varphi_a-k)}+\Gamma_b e^{i(\varphi_b+k)}+\Gamma_c)\Delta}{\sqrt{\Delta^2-(E+\xi)^2}} \\ -\frac{(\Gamma_a e^{-i(\varphi_a-k)}+\Gamma_b e^{-i(\varphi_b+k)}+\Gamma_c)\Delta}{\sqrt{\Delta^2-(E+\xi)^2}} & (E+\xi)\left(1+\frac{\sum_j \Gamma_j}{\sqrt{\Delta^2-(E+\xi)^2}}\right) \end{pmatrix} \quad \text{if } |E+\xi| < \Delta, \tag{23}$$

$$L_0(\xi,k) = \begin{pmatrix} (E+\xi)\left(1+\frac{i\sum_j \Gamma_j}{\sqrt{(E+\xi)^2-\Delta^2}}\right) & -\frac{i(\Gamma_a e^{i(\varphi_a-k)}+\Gamma_b e^{i(\varphi_b+k)}+\Gamma_c)\Delta}{\sqrt{(E+\xi)^2-\Delta^2}} \\ -\frac{i(\Gamma_a e^{-i(\varphi_a-k)}+\Gamma_b e^{-i(\varphi_b+k)}+\Gamma_c)\Delta}{\sqrt{(E+\xi)^2-\Delta^2}} & (E+\xi)\left(1+\frac{i\sum_j \Gamma_j}{\sqrt{(E+\xi)^2-\Delta^2}}\right) \end{pmatrix} \quad \text{if } |E+\xi| > \Delta. \tag{24}$$

They depend explicitly on the quasiparticle Floquet energy E, but only via the combination $E + m\omega_0$, where $\omega_0 = eV/\hbar$. This allows us to interpret Eq. (15) as the Schrödinger equation for a 1D Floquet tight-binding Hamiltonian that contains a fictitious uniform electric field ω_0, related to the energy $-m\omega_0$ of the Cooper pairs transmitted by Andreev reflection in the superconducting leads. For such tight-binding models [37,38], the energy spectrum consists of several Wannier-Stark ladders, each containing equally spaced levels separated by $\hbar\omega_0$. In addition, for the superconducting QD of interest, the Floquet states are connected by multiple Andreev reflections to the superconducting quasiparticle continua in the leads if $|E + m\omega_0| > \Delta$ (with Δ the superconducting gap). This provides a finite lifetime (or equivalently a finite spectral width) to the FWS resonances [33,34].

IV. ADIABATIC APPROXIMATION

A. Zero-voltage limit

In a three-terminal superconducting QD, the condition for the emergence of quartets is set by commensurate voltage biasing $(V_a, V_b, V_c) = (V, -V, 0)$ on the superconducting leads S_a, S_b, and S_c [28]. The matrices $M_0(m)$ and $M_\pm(m)$ no longer depend on m in the "classical" limit $V = 0$. We can then use the Bloch theorem to solve Eq. (15), which produces plane-wave solutions $\Psi_m = \exp(ikm/2)\Psi$. The wave vector k appears as a free parameter, and it can be physically interpreted by noting that the adiabatic approximation for the time-dependent problem becomes exact if $V \to 0$. These plane-wave solutions correspond to the quasiparticle operators for *static* Bogoliubov–de Gennes Hamiltonians with the superconducting order-parameter phases given by

$$\varphi_j(k) = \varphi_j + s_j k, \tag{25}$$

where $s_j = \pm 1, 0$ according to the voltage $V_j = \pm V, 0$ on lead S_j. The doublet of ABS bands has then the energy-dispersion relation $E = \pm E_A(k)$, which is a 2π-periodic function of the analogous wave vector k. The first task here is to calculate this dispersion relation, including self-energy corrections due to the reservoirs. It is easy to show that it is determined by solving the equation

$$\det(L_0(\xi = 0, k)), \tag{26}$$

where $E = \pm E_A(k)$ lies inside the superconducting gap, so Eq. (23) has to be used to define the two by two matrix L_0.

B. Andreev bound-state dispersion relation

In our three-terminal setting biased in the quartet configuration, Eq. (26) takes the form

$$f(x) = \pm\frac{|\Gamma(k)|}{\Delta} \tag{27}$$

with $x = E_A(k)/\Delta$, $f(x) = x(\sqrt{1-x^2}+c)$, $c = \sum_j \Gamma_j/\Delta$, and $\Gamma(k) = \Gamma_a e^{i(\varphi_a-k)} + \Gamma_b e^{i(\varphi_b+k)} + \Gamma_c$, using a gauge in which $\varphi_c = 0$. This provides an implicit determination of $E_A(k)$. Since this equation is valid inside the BCS gap in the reservoirs, it requires that $|x| < 1$. When x increases from 0, $f(x)$ first increases, it reaches a maximum at $x = x_M$, and then decreases until $x = 1$. Explicitly, $x_M = \sqrt{4 - c^2 + c\sqrt{8+c^2}}/\sqrt{8}$. In the tunnel limit, $c \ll 1$, $x_M \simeq \sqrt{2}/2$. We have the useful inequality

$$0 < \frac{|\Gamma(k)|}{\Delta} \leqslant c = f(1). \tag{28}$$

Note that $|\Gamma(k)|/\Delta = c$ only if $\exp(i(\varphi_a - k)) = 1 = \exp(i(\varphi_b + k))$, which implies that $\varphi_q = \varphi_a + \varphi_b = 0 \bmod 2\pi$. When $\varphi_q \neq 0 \bmod 2\pi$, for any k, there is a unique solution to Eq. (27) with $0 < x(k) < x_M$. Some examples of ABS dispersion relations are shown by the magenta curves in panels (b) and (d) of Fig. 4 in the Appendix.

In the tunnel limit, when $\Gamma_j \ll \Delta$, solutions of Eq. (27) satisfy $|x(k)| \ll 1$, and $f(x)$ can be well approximated by its tangent near the origin, i.e., $f(x) \simeq cx$. This approximation amounts to neglecting the energy dependence of self-energy corrections, at least in the subgap region, and we will use it quite often in the following discussions. This corresponds to making the following approximation:

$$L_0(\xi = 0, k) \simeq \begin{pmatrix} (1+c)E & -\Gamma(k) \\ -\Gamma(k)^* & (1+c)E \end{pmatrix}. \tag{29}$$

In this case, Eq. (27) becomes

$$E_A(k) = \pm\frac{|\Gamma(k)|}{1+c}. \tag{30}$$

The gap between the two Andreev bound-state bands closes when there is at least one value of k such that $x(k) = 0$, which requires $\Gamma(k) = 0$. For this to happen, the triangular inequality $|\Gamma_a - \Gamma_b| \leqslant \Gamma_c \leqslant \Gamma_a + \Gamma_b$ has to be satisfied (see the shaded inner triangle in Fig. 2). If this is the case, there are two angles α and β, lying in $]-\pi, \pi[$, whose values depend on Γ_j's, such that $x(k) = 0$ if and only if $(\varphi_a - k, \varphi_b + k) = \pm(\alpha, \beta)$. This shows that, generically (precisely when $\Gamma_a \neq \Gamma_b$), the gap

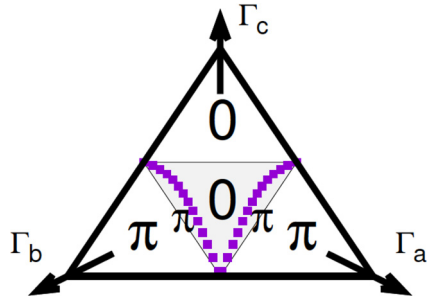

FIG. 2. Ternary diagram for the gap closing condition: The nodal lines, displayed in magenta and calculated for $\varphi_q/2\pi = 0.2$, represent the values of the parameters for which the gap between the two Andreev bound-state bands vanishes [see Eq. (31)]; below these two lines, the Berry phase takes the value $\varphi_B = \pi$. The smaller shaded inner triangle shows all the possible values of the nodal lines when $0 < \varphi_q/2\pi < 1$.

closes for two different values of $\varphi_q = \pm(\alpha + \beta)$. For each of them, there is a unique value of k such that $x(k) = 0$. The gap closes at $\varphi_q = 0 \bmod 2\pi$ if $\Gamma_a = \Gamma_b$ and $\alpha + \beta = 0 \bmod 2\pi$, and there are two values of k such that $x(k) = 0$. This gap closing condition can be formulated as follows in the generic case $\Gamma_a \neq \Gamma_b$ or $\varphi_q \neq 0 \bmod 2\pi$: the gap closes if $\Gamma_c = \Gamma_c^{(0)}$, with

$$\Gamma_c^{(0)} = \frac{\left|\Gamma_a^2 - \Gamma_b^2\right|}{\sqrt{\Gamma_a^2 + \Gamma_b^2 - 2\Gamma_a\Gamma_b\cos\varphi_q}}. \tag{31}$$

This relation is represented by the magenta data points in Fig. 2.

C. Floquet energies in the adiabatic limit

In the adiabatic limit, the solution of the time-dependent Bogoliubov–de Gennes Eq. (4) is well approximated by

$$\Gamma^\dagger(t) = e^{-i\varphi(t)}\Gamma_A^\dagger(t), \tag{32}$$

where $\Gamma_A^\dagger(t)$ is a quasiparticle creation operator associated with the Andreev bound state for the Hamiltonian $H(t)$. This means that $\Gamma_A^\dagger(t)$ satisfies

$$[H(t), \Gamma_A^\dagger(t)] = E_A(t)\Gamma_A^\dagger(t). \tag{33}$$

The physical time variable t is directly related to the wave vector k discussed earlier by $k = 2\omega_0\, t = \omega_J\, t$. As usual [4], the phase factor $\varphi(t)$ is the sum of two contributions, a dynamical phase φ_d and a geometrical phase φ_g. As always,

$$\varphi_d = \frac{1}{\hbar}\int_0^t E_A(t')\,dt'. \tag{34}$$

The geometrical phase φ_g depends generically on an arbitrary choice of phases for the instantaneous quasiparticle operators $\Gamma_A^\dagger(t)$, excepted when the system Hamiltonian at time t is the same as at $t = 0$, in particular when t is equal to the Josephson period $T_J = 2\pi/\omega_J$. In this case, φ_g is gauge-invariant, and is an example of a Berry phase φ_B.

To evaluate this Berry phase, we have to describe in more detail how the quasiparticle operators $\Gamma_A^\dagger(k)$ vary as k evolves from $-\pi$ to π. We write

$$\Gamma_{A\sigma}^\dagger(k) = u(k)d_\sigma^\dagger + \sigma\, v(k)d_{-\sigma} + \cdots, \tag{35}$$

where the dots refer to virtual contributions from the superconducting reservoirs, and the spinor $\chi(k) = (u(k), v(k))^T$ is a null eigenvector for $L_0(\xi = 0, k)$, i.e., $L_0(\xi = 0, k)\chi(k) = 0$, with $E = E_A(k)$ in $L_0(\xi = 0, k)$. From Eq. (29), we see that the Nambu spinor $\chi(k)$ associated with the dot is subjected to a fictitious magnetic field lying in the x-y plane and oriented along $\Gamma(k)$ (after identifying complex numbers with points in the x-y plane in the usual way). As k runs from $-\pi$ to π, $\Gamma(k)$ describes an ellipse $\mathcal{E}$ around the origin of the complex plane. For such a closed path, the winding number w is defined as

$$\alpha(\pi) - \alpha(-\pi) = 2\pi w, \tag{36}$$

where $\Gamma(k) = |\Gamma(k)|e^{i\alpha(k)}$. Correspondingly, the pseudospin associated with the Nambu spinor $\chi(k)$ performs w turns around the equator on the Bloch sphere, which induces a Berry phase $\varphi_B \equiv -w\pi$ [4]. The appearance of Berry phases in multicomponent WKB equations has been pointed out by many authors, both in the mathematics [39] and physics [40,41] communities. In this specific model, when the dot level lies exactly at zero energy, φ_B takes only two values: 0 or π modulo 2π.

At this point, we should emphasize that this quantization is not robust. A finite gate voltage acting on the dot adds a term proportional to the Pauli matrix σ^z in $L_0(\xi = 0, k)$. As a result, the spinor $\chi(k)$ is no longer confined to the equator, but to a constant altitude circle on the Bloch sphere. In this situation, the Berry phase is now equal to $w\zeta$, where $\zeta = \pi$ at zero gate voltage, and it departs from π linearly at small gate voltage.

We have $w = 0$ so $\varphi_B = 0$ when the origin of the complex plane is not inside the ellipse $\mathcal{E}$, and $w = \pm 1$ so $\varphi_B = \pm\zeta$ otherwise. This implies that φ_B jumps from 0 to $\pm\zeta$, precisely at the point in parameter space where the minimum over k of $|\Gamma(k)|$ vanishes. Interestingly, we always have $\varphi_B \equiv \pm\zeta$ in the two-terminal case, so that the third terminal biased is necessary in order to observe the jump of the Berry phase from $\pm\zeta$ to 0.

A cautious reader may worry that the Berry phase might be sensitive to virtual contributions from the superconducting reservoirs, whose existence is reminded by the dots in Eq. (35). In fact, such virtual contributions are fully taken into account through the self-energies, which appear in the expression (23) for $L_0(\xi, k)$. So the previous discussion of the Berry phase does take into account these virtual contributions.

The Berry phase φ_B manifests itself on the Floquet spectrum, as we request that the quasiparticle operator $\Gamma^\dagger(t)$ should satisfy the periodicity condition

$$\Gamma^\dagger(t + T_J) = e^{-iET_J}\Gamma^\dagger(t). \tag{37}$$

This leads to

$$\varphi_d(T_J) + \varphi_B = ET_J + 2\pi n, \tag{38}$$

where n is an arbitrary integer. Because $\varphi_d(T_J) = \langle E_A\rangle T_J$, where $\langle E_A\rangle$ denotes the Andreev bound-state energy averaged

over one period, this leads to the following Bohr-Sommerfeld-type formula:

$$E = \langle E_A \rangle - \left(2n + w\frac{\zeta}{\pi}\right)\omega_0. \tag{39}$$

Because of the charge conjugation symmetry of the Bogoliubov–de Gennes equations, applying Hermitian conjugation to $\Gamma^\dagger(t)$ produces a second Wannier-Stark ladder in which E is replaced by $-E$ modulo ω_J. At the level of the adiabatic approximation presented in this subsection, these two Wannier-Stark ladders remain decoupled.

D. Floquet spectrum beyond the adiabatic limit

Going beyond the adiabatic approximation does induce some coupling, and physically this coupling corresponds to Landau-Zener transitions between the two Andreev bound-state bands. A natural way to capture them is to go back to the general Floquet formulation presented in Sec. III. At small dc voltage bias, the linear potential term $m\omega_0$ entering in Eqs. (7)–(10) is small, so the difference equation (15) can be treated by the WKB method. Since this is a standard method, and given that explicit calculations are a bit tedious, we have relegated this contribution to the Appendix. Interestingly, the shift in the Floquet spectra induced by a nontrivial Berry phase is still present at intermediate voltages (compared to the superconducting gap). To cover the full range of possible voltages, a full numerical calculation is necessary, the results of which will be presented in Fig. 3 below.

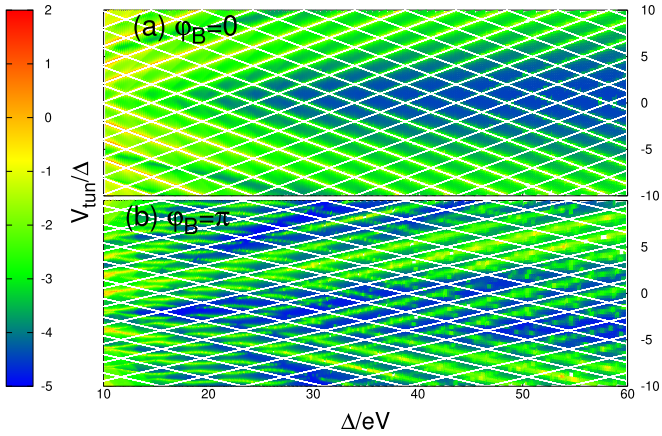

FIG. 3. Tunnel spectroscopy of the Berry phase: The figure features the logarithm of the local density of states on the quantum dot (in color scale) as a function of inverse voltage Δ/eV (x-axis) and tunnel probe bias voltage $eV_{\rm tun}/\Delta$ (y-axis). The Berry phase is $\varphi_B = 0$ in panel (a) and $\varphi_B = \pi$ in panel (b). The tunnel spectra reveal the Floquet-Wannier-Stark ladders, and they are compared to the tilted white lines, which correspond to $w = 0$ in Eq. (39). The half-a-period shift appearing in panel (b) is a signature of the nontrivial Berry phase $\varphi_B = \pi$, while $\varphi_B = 0$ for the nonshifted tunnel spectrum in panel (a). The three-terminal superconducting QD has $\Gamma_a/\Delta = 0.4$, $\Gamma_b/\Delta = 0.2$, and $\varphi_q = 0$, with (a) $\Gamma_c/\Delta = 1.0$ and (b) $\Gamma_c/\Delta = 0.3$.

V. TUNNELING SPECTRA CALCULATIONS

Here, we would like to illustrate our prediction by exploring the FWS ladder spectra under the presence of the nontrivial Berry phase. We evaluate the spectra that could possibly be measured in a superconducting multiterminal quantum dot with an additional tunneling probe, as depicted in Fig. 1.

A. Tunneling density of states

One way to detect FWS ladders is to perform local tunneling spectroscopy on the dot. For this, we tunnel-couple a normal probe to the quantum dot. The differential tunneling conductance is given by

$$\frac{\partial I_{\rm tun}(t)}{\partial V_{\rm tun}} = -e^2\int_{-\infty}^{\infty}\frac{d\omega}{2\pi}J^2_{\rm tun}(\omega)f'_{\rm FD}(\omega + eV_{\rm tun}) \times \sum_n i\left[G^R_d(\omega)_n - G^R_d(\omega)^*_{-n}\right]e^{-in\omega_0 t}. \tag{40}$$

Here, $J^2_{\rm tun}(\omega)$ is the Fermi golden rule squared tunneling amplitude times the density of states in the normal probe at energy ω, and $f'_{\rm FD}(\omega)$ is the derivative of the Fermi-Dirac distribution. Because of the periodic time dependence of the BCS Hamiltonian, the tunneling current $I_{\rm tun}(t)$ is also periodic in time. $G^R_d(\omega)_n$ is the Fourier transform of the retarded Green's function on the dot, defined explicitly as

$$G^R_d(t,t') = \int_{-\infty}^{\infty}\frac{d\omega}{2\pi}\sum_n G^R_d(\omega)_n e^{-i\omega(t-t')}e^{-in\omega_0 t}. \tag{41}$$

In fact, $G^R_d(\omega)_n$ is directly related to the resolvent operator defined earlier through $G^R_d(\omega)_n = \mathcal{R}(\omega)_{n,0}$. The dc tunneling current takes a particularly simple form,

$$\frac{\partial I_{\rm tun}}{\partial V_{\rm tun}} = 2e^2\int_{-\infty}^{\infty}\frac{d\omega}{2\pi}J^2_{\rm tun}(\omega)f'_{\rm FD}(\omega + eV_{\rm tun}){\rm Im}G^R_d(\omega)_{n=0}. \tag{42}$$

Finally, in the zero-temperature limit, we obtain

$$\frac{\partial I_{\rm tun}}{\partial V_{\rm tun}} = -2e^2J^2_{\rm tun}(-eV_{\rm tun}){\rm Im}G^R_d(\omega)_{n=0}. \tag{43}$$

B. Numerical results

These results raise the question of the possible experimental observation of these effects. Recently, we have shown that finite frequency noise measurements provide experimental access to differences $E_n - E_{n'}$ between two FWS quasienergy eigenvalues [34]. This is interesting to evidence level repulsion induced by Landau-Zener-Stückelberg interladder tunneling processes, but this noise spectroscopy is not sensitive to the global shift of the FWS spectrum induced by Berry phase jumps. Therefore, we propose to perform tunnel spectroscopy on the quantum dot [see Fig. 1(a)]. The differential dc-tunnel conductance through the dot directly probes the FWS ladder density of states. Figure 3 shows two tunnel spectra, one for $\varphi_B = 0$ [panel (a)] and the other for $\varphi_B = \pi$ [panel (b)]. The global shift associated with a Berry phase jump is clearly visible in Fig. 3 while comparing in both cases the numerical tunnel spectra to the tilted reference white line corresponding to $w = 0$ in Eq. (39). For further details on the numerical

calculation of the resolvent, see Sec. III in the Supplemental Material [44].

VI. SUMMARY AND PERSPECTIVES

To conclude, we have shown that, in superconducting multiterminal QDs, a nontrivial Berry phase φ_B can appear on the quartet line at commensurate voltages. Via semiclassical calculations, we have demonstrated that the parameter space splits into two regions with $\varphi_B = 0$ or $\varphi_B = \pi$, separated by a hypersurface on which the gap between the Andreev bands closes. We have seen that the FWS spectrum is controlled by the Berry phase. The nontrivial Berry phase can be revealed by probing the density of states of the quantum dot in a tunneling spectroscopy experiment. Our numerical calculations directly show that the FWS ladder spectra are shifted by half a period when $\varphi_B = \pi$, as compared to $\varphi_B = 0$. While our calculations are performed when the superconducting quantum dot level sits at zero energy, one may expect to continuously tune the Berry phase by changing the energy of the dot, for example via electrostatic gating.

ACKNOWLEDGMENTS

The authors thank the Centre Régional Informatique et d'Applications Numériques de Normandie (CRIANN) for use of its facilities. The authors thank the Infrastructure de Calcul Intensif et de Données (GRICAD) for use of the resources of the Mésocentre de Calcul Intensif de l'Université Grenoble-Alpes (CIMENT). B.D. and R.M. acknowledge fruitful discussions with Y. Colin de Verdière, F. Faure, and A. Joye. R.D. and R.M. acknowledge financial support from the Centre National de la Recherche Scientifique (CNRS) and Karlsruhe Institute of Technology (KIT), through the International Laboratory "LIA SUPRADEVMAT" between the Grenoble and Karlsruhe campuses. This work was partly supported by Helmholtz society through program STN and the DFG via the projects DA 1280/3-1.

APPENDIX A: LOCAL SEMICLASSICAL SOLUTIONS

1. General idea

A small bias voltage V plays formally the role of Planck's constant $\hbar$ in the Wentzel-Kramers-Brillouin (WKB) approximation [42]. The classical limit $\hbar \to 0$ in standard quantum mechanics corresponds to $eV/\Delta \to 0$ in superconducting QDs. The semiclassical approximation for $eV \ll \Delta$ in superconducting junctions was pioneered by Bratus *et al.* [43]. In this approximation, the wave vector k has slow variations with m. Let us first transform m into a continuous variable via

$$\epsilon = 2\omega_0, \quad m\omega_0 = \xi, \tag{A1}$$

where ϵ is a small parameter. Equation (15) reads

$$M_0(\xi)\Psi(\xi) - M_+\left(\xi + \frac{\epsilon}{2}\right)\Psi(\xi+\epsilon) - M_-\left(\xi - \frac{\epsilon}{2}\right)\Psi(\xi-\epsilon) = 0. \tag{A2}$$

The semiclassical ansatz takes the form

$$\Psi(\xi) = e^{i\frac{\theta(\xi)}{\epsilon}}\chi(\xi), \tag{A3}$$

where $\chi(\xi)$ can be expanded in ϵ according to

$$\chi(\xi) = \sum_{n=0}^{\infty} \epsilon^n \chi_n(\xi). \tag{A4}$$

Assuming that $\theta(\xi)$ and $\chi(\xi)$ have infinitely many derivatives, we can view the linear operator acting on $\chi(\xi)$ in Eq. (A2) as a differential operator L of infinite order, which can also be expanded in ϵ according to

$$L = \sum_{n=0}^{\infty} \epsilon^n L_n. \tag{A5}$$

This leads to an infinite set of equations, from which we keep the first two of lowest order:

$$L_0\chi_0(\xi) = 0, \tag{A6}$$

$$L_0\chi_1(\xi) + L_1\chi_0(\xi) = 0. \tag{A7}$$

2. Classical phase-space trajectories

Let us first consider the zeroth-order Eq. (A6):

$$L_0(\xi, \theta'(\xi))\chi_0(\xi) = 0, \tag{A8}$$

where

$$L_0(\xi, \theta'(\xi)) = M_0(\xi) - M_+(\xi)e^{i\theta'(\xi)} - M_-(\xi)e^{-i\theta'(\xi)} \tag{A9}$$

is a 2×2 matrix. The L_0 operator acts on $\chi_0(\xi)$ only through pointwise multiplication, i.e., it does not involve any differential operator involving the ξ variable. Equation (A6) has nontrivial solutions if $\det L_0(\xi, k) = 0$, namely

$$\det(M_0(\xi) - M_+(\xi)e^{i\theta'(\xi)} - M_-(\xi)e^{-i\theta'(\xi)}) = 0. \tag{A10}$$

In the general spirit of semiclassical (or WKB) approximation, we introduce the ξ-dependent wave number $k(\xi)$ by $k(\xi) = \theta'(\xi)$. Equation (A10) determines a curve in the (ξ, k) plane called the *classical trajectory* in *phase space*. Recalling that, in Eq. (15), E and m enter only through the combination $E + m\omega_0$, we see that E and ξ enter Eq. (A10) only through $E + \xi$. As a result, this classical trajectory is related in a very simple manner to the Andreev subband energy-dispersion relation $E_A(k)$ by

$$E + \xi = \sigma E_A(k), \tag{A11}$$

where $\sigma = \pm 1$ labels the two Andreev subbands. In Eq. (A11), the total energy E is the sum of the "kinetic term" $\sigma E_A(k)$ arising from the ABS dispersion relation, and the "potential term" $-\xi$ resulting from dc-voltage biasing. Here, the (ξ, k) variables are seen as the equivalent position-momentum phase space of a fictitious spin-1/2 particle. For a given choice of E and σ, Eq. (A11) defines a curve $\mathcal{T}_{E,\sigma}$ in this (ξ, k) plane, which we call the "classical trajectory" in phase space. If k is used as a parameter, Eq. (A11) implies that $\xi(k)$ is simply given by the ABS dispersion relation, up to a shift of ξ by $-E$. In the time-dependent picture, we have $k = \omega_0 t$, and ξ is a periodic function of time, as expected for Bloch oscillations in the solid-state analog [33,34].

Because of Heisenberg's uncertainty principle, a small bias voltage induces quantum fluctuations $\Delta\xi\, \Delta k \sim eV$ around

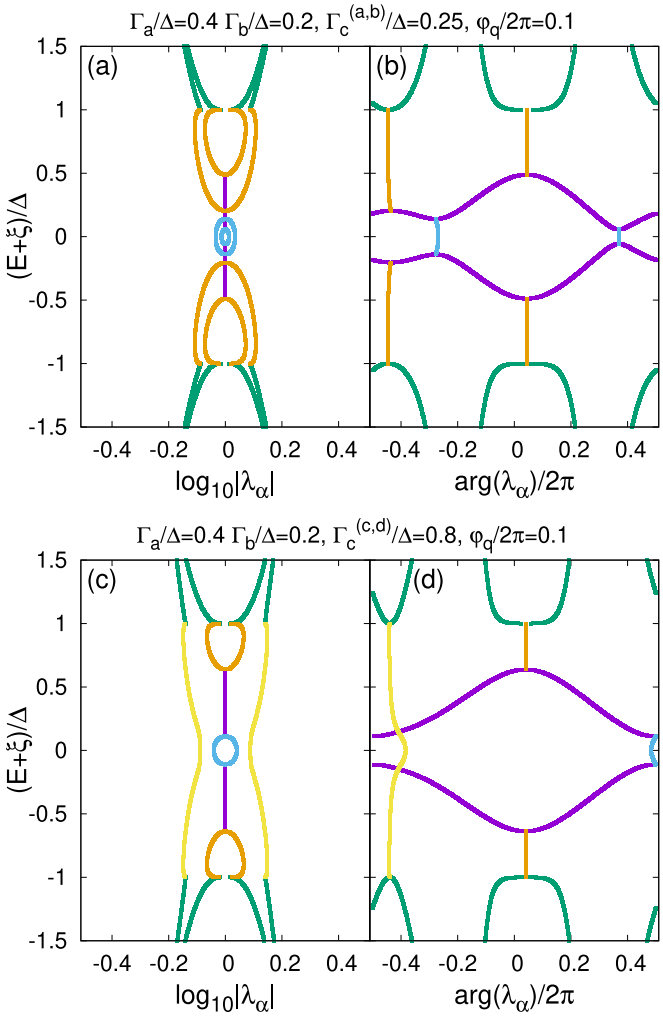

FIG. 4. Classical trajectories: The figure shows the classical trajectory $\mathcal{T}_{E,\pm}$, together with the tunneling paths, i.e., the four complex solutions k_α of Eq. (A11), each with a given value of $E+\xi$. In these plots, we use the complex variable $\lambda_\alpha = \exp(ik_\alpha)$. Panels (a), (c) and (b), (d) show, respectively, $\log_{10}|\lambda_\alpha|$ and $\arg(\lambda_\alpha)/2\pi$ on the x-axis. The y-axis in each panel features $E+\xi$ normalized to the gap Δ. The dispersion relation $E_A(k)$ (in magenta) has two local minima and two local maxima $\mathcal{N}^{(a,b)} = 2$ in panel (b), as k varies in the interval $-\pi < k < \pi$. Panel (d) corresponds to a single local minimum and maximum $\mathcal{N}^{(c,d)} = 1$. The color code is explained in the text.

the classical trajectories, and it also produces Landau-Zener-Stückelberg transitions between the two Andreev bands. In the semiclassical approximation, Landau-Zener tunneling is captured by paths connecting both classical trajectories $\mathcal{T}_{E,+}$ and $\mathcal{T}_{E,-}$. Along these tunneling paths, ξ is still a real number but k becomes complex, as is expected for evanescent wave functions in tunneling processes.

The classical trajectories and the tunneling paths are displayed in Fig. 4. Two representative sets of parameters are used in Figs. 4(a) and 4(b) and Figs. 4(c) and 4(d), differing by the value of Γ_c/Δ [i.e., $\Gamma_c^{(a,b)}/\Delta = 0.25$ in panels (a), (b) and $\Gamma_c^{(c,d)}/\Delta = 0.8$ in panels (c), (d)], all other parameters being the same for all panels (i.e., $\Gamma_a/\Delta = 0.4$, $\Gamma_b/\Delta = 0.2$, and $\varphi_q/2\pi = 0.1$). Here, $\Gamma_j = J_j^2/W$ stands from the contact transparency between the dot and superconducting reservoir

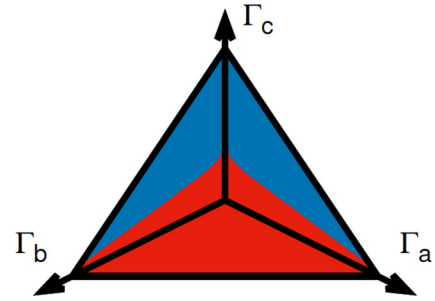

FIG. 5. Ternary diagrams for the number of minima in $E_A(k)$: the domain in parameter space in which the dispersion relation for $\mathcal{N} = 1$ and 2 minima is shown in blue and red, respectively, for $\varphi_q/2\pi = 0.2$.

j, where J_j is the corresponding tunnel amplitude and W is the bandwidth. The variable $\varphi_q = \varphi_a + \varphi_b - 2\varphi_c$ denotes the time-independent quartet phase.

In all the panels [(a)–(d)] of Fig. 4, the y-axis is $E+\xi$ [see Eq. (A11)]. On the x-axis, panels (a) and (c) feature $\log_{10}|\lambda_\alpha|$ and panels (b) and (d) show $\arg(\lambda_\alpha)/2\pi$, where $\lambda_\alpha = \exp(ik_\alpha)$. The set of solutions to the discrete homogeneous Eq. (15) has dimension 4. Then, for each choice of ξ, there are four real or complex solutions $k(\xi) \bmod 2\pi$ of $\det L_0(\xi, k) = 0$. The magenta curves in Figs. 4(a)–4(d) correspond to ξ and k taking real values, thus with $\log_{10}|\lambda_\alpha| = 0$. In panels (b) and (d), the magenta data points coincide with the ABS dispersion relations $\pm E_A(k)/\Delta$. The $|E+\xi| > \Delta$ branches in green in Figs. 4(a)–4(d) have complex k values, due to the coupling of the dot level to the quasiparticle continua above the superconducting gap in the leads. The tunneling paths between the two ABSs are shown in blue. Those between the ABS and quasiparticle branches are shown in orange. The tunneling paths connecting the two continua at energies $E+\xi < -\Delta$ and $E+\xi > \Delta$ are shown in yellow in panels (c) and (d).

The number $\mathcal{N}$ of local minima and maxima in the dispersion relation $E_A(k)$ changes from $\mathcal{N}^{(a,b)} = 2$ to $\mathcal{N}^{(c,d)} = 1$ as Γ_c/Δ increases from $\Gamma_c^{(a,b)}/\Delta$ [panels (a),(b)] to $\Gamma_c^{(c,d)}/\Delta$ [panels (c),(d)]. The values $\mathcal{N} = 1, 2$ coincide with the number of tunneling loops between the two Andreev bands. Indeed, two tunneling loops or a single tunneling loop can be visualized in blue in Fig. 4(a) or Fig. 4(c). The jump in $\mathcal{N}$ defines a hypersurface in the three-dimensional parameter space $(\Gamma_a/\Gamma_c, \Gamma_b/\Gamma_c, \varphi_q)$, separating the two regions with $\mathcal{N} = 1, 2$. A representative constant-φ_q section of this parameter space is shown in Fig. 5.

3. $\mathcal{N} = 1$ to 2 transition

Now we provide more details on the determination of $\mathcal{N}$ and of the boundary between $\mathcal{N} = 1$ and 2 regions in parameter space. Equation (27) shows that it is useful to specify the variations of $|\Gamma(k)|$ when k varies from $-\pi$ to π. The Fourier series $|\Gamma(k)|^2$ contains harmonics of the form e^{imk} for $|m| \leqslant 2$, therefore we have two possibilities: either $|\Gamma(k)|^2$ has two minima and two maxima in $[-\pi, \pi]$ ($\mathcal{N} = 2$), or it has only one minimum and one maximum ($\mathcal{N} = 1$). In the former case, as ξ increases across a given classically allowed

region, the number of real $k(\xi)$ values is equal to 2, next 4, and then 2 again. An illustration of this situation is shown in Fig. 4(b). In the latter case, the number of real $k(\xi)$ values is only 2 throughout each classically allowed region. This shows that for any value of ξ, there are at least two $k(\xi)$ values that are not real. Thus, we obtain a qualitatively simpler situation in which two complex branches of solutions are decoupled from the real classical trajectory, as shown by the yellow lines in panels (c) and (d) of Fig. 4.

These two possible regions with $\mathcal{N}=1$, 2 are separated by a hypersurface in the three-dimensional parameter space $(\Gamma_a/\Gamma_c,\ \Gamma_b/\Gamma_c,\ \varphi_q)$. Its equation is obtained by imposing that the first and second derivatives of $|\Gamma(k)|^2$ vanish simultaneously, which is equivalent to the vanishing of the result for two degree-4 polynomials. A simple geometric interpretation for this hypersurface can be obtained, in spite of the rather complex corresponding equation. When k varies, $\Gamma(k)$ moves along an ellipse $\mathcal{E}$ in the complex plane. An extremum of $|\Gamma(k)|^2$ occurs when the origin lies on the normal to $\mathcal{E}$ at the $\Gamma(k)$ point. At the $\mathcal{N}=1$ to 2 transition point, a minimum and a maximum of $|\Gamma(k)|^2$ collide, so the origin belongs to the intersection of infinitely close normals, i.e., it is the curvature center of $\mathcal{E}$ at $\Gamma(k)$. So the $\mathcal{N}=1$ to 2 transition occurs when the origin lies on the evolute of $\mathcal{E}$.

4. Dissipative high-energy branches

Because of the coupling of the dot levels to quasiparticle continua, we have two complex branches with $\mathrm{Im}k>0$, which correspond to quickly decreasing solutions at large ξ, and two branches with $\mathrm{Im}k<0$, which generate growing solutions. On physical grounds, the resolvent operator $\mathcal{R}(E)$ will be built from solutions that decay as $\xi\to\pm\infty$, so we have to choose the branches with $\mathrm{Im}k>0$ as $\xi\to\infty$ and with $\mathrm{Im}k<0$ as $\xi\to-\infty$. Let us describe the former with the simplifying assumption that $E+\xi\gg\Delta$. From the explicit form of L_0 given in Eq. (24), we see that, in this regime, the equation $\det L_0(\xi,k)=0$ simplifies and becomes

$$\exp(2ik)=-\frac{\Delta^2\Gamma_a\Gamma_b}{(E+\xi)^4}\exp\left(i(\varphi_a-\varphi_b)\right), \tag{A12}$$

which leads to

$$k=\sigma\frac{\pi}{2}+\frac{\varphi_a-\varphi_b}{2}+i\ln\left(\frac{(E+\xi)^2}{\sqrt{\Gamma_a\Gamma_b}\Delta}\right),\quad \sigma=\pm1. \tag{A13}$$

The leading exponential factor in these decaying solutions is

$$\exp\left\{-\frac{|E+\xi|}{\epsilon}\left[\ln\left(\frac{(E+\xi)^2}{\sqrt{\Gamma_a\Gamma_b}\Delta}\right)-2\right]\right\}. \tag{A14}$$

Exactly at the BCS gap, i.e., if $E+\xi=\pm\Delta$, Eq. (A10) simplifies into

$$\Gamma(k)\Gamma(k^*)^*=\left(\sum_j\Gamma_j\right)^2. \tag{A15}$$

This equation has no real k solution unless $\varphi_q=0$, and thus the vicinity of the BCS gap then lies in the classically forbidden regions. For further details on the reflections induced at gap edges, see Sec. I in the Supplemental Material [44].

5. Nondegeneracy condition

Let us consider Eq. (A8). This equation has nontrivial solutions $\chi_0(\xi)$ when $(\xi,k=\theta'(\xi))$ lies on the classical trajectory (extended to complex k-values). *A priori*, two cases are possible. Generically, when $\det L_0(\xi,k)=0$, the rank of $L_0(\xi,k)$ is equal to unity, so that the direction of the two-component spinor $\chi_0(\xi)$ is unambiguously determined. We therefore associate a line in $\mathbb{C}^2$ to each point $(\xi,k)\in\mathbb{R}\times\mathbb{C}$ such that $L_0(\xi,k)$ is of rank 1. A less common possibility is that the rank of $L_0(\xi,k)$ is equal to 0, i.e., $L_0(\xi,k)=0$. For this to happen, we need to have simultaneously $E+\xi=0$ and $\Gamma(k)=\Gamma(k^*)^*=0$. Setting $\lambda=e^{ik}$, this happens when the polynomials $P(\lambda)=\Gamma_b e^{i\varphi_b}\lambda^2+\Gamma_c\lambda+\Gamma_a e^{i\varphi_a}$ and $Q(\lambda)=\Gamma_a^* e^{-i\varphi_a}\lambda^2+\Gamma_c^*\lambda+\Gamma_b^* e^{-i\varphi_b}$ have at least one common root. A necessary and sufficient condition for this to happen is that their resultant R vanishes, which reads explicitly

$$R=\left(\Gamma_a^2-\Gamma_b^2\right)^2-\Gamma_c^2\left(\Gamma_a^2+\Gamma_b^2-2\Gamma_a\Gamma_b\cos\varphi_q\right)=0. \tag{A16}$$

A little algebra shows that $R=0$ is possible in two situations: either the gap between the two Andreev bands closes, or the gap does not close but we have $\Gamma_a=\Gamma_b<\Gamma_c/2$ and $\cos\varphi_q=1$. Except for these particular cases, the solutions of Eq. (A8) define a smooth line bundle $\mathcal{B}$ over the classical trajectory $\mathcal{C}$ (extended to complex k values).

Let us choose a smooth local frame $e(\xi,k(\xi))$ for this bundle, i.e., a smooth solution of $L_0(\xi,k(\xi))e(\xi,k(\xi))=0$. To lowest order in the small ϵ parameter, local semiclassical solutions have the form $\chi_0(\xi)=f(\xi)e(\xi,k(\xi))$ for so far unknown smooth scalar functions $f(\xi)$, i.e., they are smooth local sections of the bundle $\mathcal{B}$. To determine $f(\xi)$ requires more information, which is provided by the first-order equation (A7).

6. Transport equation

To simplify the discussion, we discard the ξ-dependence in $M_\pm(\xi)$ by using the approximate forms

$$M_0(\xi)=\begin{pmatrix}(E+\xi)(1+c) & -\Gamma_c\\ -\Gamma_c & (E+\xi)(1+c)\end{pmatrix}, \tag{A17}$$

$$M_+(\xi)=\begin{pmatrix}0 & \Gamma_b e^{i\varphi_b}\\ \Gamma_a e^{-i\varphi_a} & 0\end{pmatrix}, \tag{A18}$$

$$M_-(\xi)=\begin{pmatrix}0 & \Gamma_a e^{i\varphi_a}\\ \Gamma_b e^{-i\varphi_b} & 0\end{pmatrix}. \tag{A19}$$

Note that M_+ and M_- are independent of ξ in this approximation. This is motivated by the observation that, as explained in Sec. IV B, self-energies barely affect the shape of the real part of the classical trajectory. With this simplification, the $L_1(\xi,k(\xi))$ operator is the following:

$$L_1=(-M_+e^{ik}+M_-e^{-ik})\frac{d}{d\xi}-\frac{i}{2}k'(\xi)(M_+e^{ik}+M_-e^{-ik}). \tag{A20}$$

It is convenient to introduce the operator $K(\xi,k(\xi))=-\frac{i}{2}(M_+e^{ik(\xi)}-M_-e^{-ik(\xi)})$. Then, using $d/d\xi=\partial/\partial\xi+k'(\xi)\partial/\partial k$, we have

$$iL_1=2K+\frac{dK}{d\xi}. \tag{A21}$$

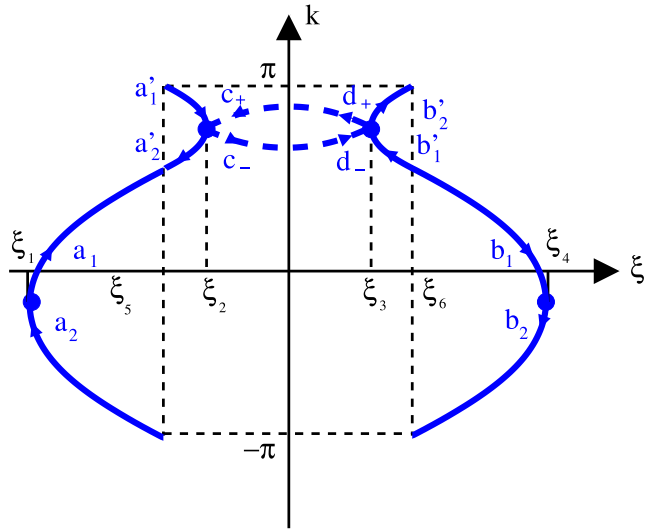

FIG. 6. Semiclassical wave function for $\mathcal{N} = 1$: The semiclassical trajectory $\mathcal{T}_{E,-}$ ($\mathcal{T}_{E,+}$) exhibits turning points at ξ_1 and ξ_2 (ξ_3 and ξ_4). The wave vector $k(\xi)$ jumps by 2π at ξ_5 and ξ_6. Classical trajectories $\mathcal{T}_{E,-}$ and $\mathcal{T}_{E,+}$ are depicted by full lines, and they are connected by a pair of tunneling paths depicted by dashed lines. Arrows near turning points indicate either an increasing phase function $\theta(\xi)$ along classical trajectories, or an increasing modulus along tunneling paths.

We also have a useful relation between K and L_0:

$$\frac{dL_0}{d\xi} = (1+c)I + 2k'(\xi)K. \tag{A22}$$

Equation (A7) imposes that $L_1\chi_0$ should be in the image of L_0, which is of rank 1 on the classical trajectory. It is convenient to introduce a left eigenvector frame $\langle e(\xi, k(\xi))|$ such that $\langle e(\xi, k(\xi))|L_0(\xi, k(\xi)) = 0$. Taking Eq. (A21) into account, the first-order equation reads

$$2\langle e|K\frac{d}{d\xi}|\chi_0\rangle + \langle e|\frac{dK}{d\xi}|\chi_0\rangle = 0. \tag{A23}$$

Geometrically, this defines a connection on the bundle $\mathcal{B}$. An explicit solution of this equation is derived in Sec. III of the Supplemental Material [44].

APPENDIX B: COUPLED FWS LADDERS

Now, we demonstrate the Bohr-Sommerfeld quantization condition for periodic orbits. Then, we solve the Landau-Zener-Stückelberg transitions between the Andreev bound-state branches with $\mathcal{N} = 1$ and 2 tunneling paths [see Figs. 2(c) and 2(d) and Figs. 2(a) and 2(b), respectively].

1. Handling open orbits

There is a domain in parameter space such that the number of real $k(\xi)$ values is only 2 throughout each classically allowed region, corresponding to $\mathcal{N} = 1$. The classical orbit is delimited by the two intervals $[\xi_1, \xi_2]$ and $[\xi_3, \xi_4]$, with $\xi_2 < \xi_3$ (see Fig. 6). Note that $2E + \xi_1 + \xi_4 = 2E + \xi_2 + \xi_3 = 0$. When k runs from $-\pi$ to π, on the left piece of the classical trajectory, ξ decreases from ξ_5 to ξ_1, forming the lower part of the $k_2(\xi)$ branch. Then ξ increases from ξ_1 to ξ_2, forming the full $k_1(\xi)$ branch. Eventually, ξ decreases from ξ_2 to ξ_5, forming the upper part of the $k_2(\xi)$ branch. Most notations are explained in Fig. 6. The semiclassical ansatz, to lowest order in ϵ, amounts to writing the wave function in $[\xi_1, \xi_2]$ as $\Psi(\xi) = \Psi_1(\xi) + \Psi_2(\xi)$, with

$$\Psi_1(\xi) = a_1 k_1'(\xi)^{1/2} e^{\frac{i}{\epsilon}\int_{\xi_1}^{\xi} k_1(\xi')d\xi'} e(\xi, k_1(\xi)), \tag{B1}$$

where $e(\xi, k(\xi))$ denotes the right zero eigenvector of $L_0(\xi, k(\xi))$ introduced in Sec. III of the Supplemental Material [44]. Because we are dealing with an *open* classical orbit, the $k_2(\xi)$ branch is discontinuous at ξ_5, with $k(\xi + \delta\xi) - k(\xi - \delta\xi) \to 2\pi$ as $\delta\xi \to 0^+$, and thus we prefer to slightly postpone the discussion of $\Psi_2(\xi)$. As usual, the turning points at ξ_1 and ξ_2 (where two branches meet) need special care. In the vicinity of ξ_1, we have $k_1(\xi) = k(\xi_1) + c(\xi - \xi_1)^{1/2} + \cdots$ and $\theta(\xi) = k(\xi_1)(\xi - \xi_1) + \frac{2c}{3}(\xi - \xi_1)^{3/2} + \cdots$, where c is a positive constant. As $\xi \overset{>}{\to} \xi_1$, we have

$$\Psi_1(\xi) \simeq \frac{a_1}{(\xi - \xi_1)^{1/4}} e^{\frac{i2c}{3\epsilon}(\xi-\xi_1)^{3/2}} \Phi_{1,\mathrm{reg}}(\xi), \tag{B2}$$

with $\Phi_{1,\mathrm{reg}}(\xi)$ a smooth function near ξ_1.

For $\Psi_2(\xi)$, we can use the same definition as Eq. (B1) for $\Psi_1(\xi)$, with $k_1(\xi)$ replaced by $k_2(\xi)$, as long as $\xi_1 \leqslant \xi \leqslant \xi_5$. Near ξ_1, we then obtain

$$\Psi_2(\xi) \simeq \frac{a_2}{(\xi - \xi_1)^{1/4}} e^{-\frac{i2c}{3\epsilon}(\xi-\xi_1)^{3/2}} \Phi_{2,\mathrm{reg}}(\xi). \tag{B3}$$

The key point here is that $\Phi_{1,\mathrm{reg}}(\xi_1) = \Phi_{2,\mathrm{reg}}(\xi_1)$, so that, as usual [42], we can match the various semiclassical wave functions near the turning point at ξ_1 using Airy functions. Imposing decay in the classically forbidden side $\xi < \xi_1$ leads to

$$a_1 = -ia_2. \tag{B4}$$

Let us for a moment neglect the tunneling processes between the two Andreev bands. We would like to apply a similar relation for the turning point at ξ_2. For this, we need the leading behavior of $\Psi_1(\xi)$ and $\Psi_2(\xi)$ near ξ_2. On the one hand, we have

$$\Psi_1(\xi) \simeq \frac{a_1'}{(\xi_2 - \xi)^{1/4}} e^{\frac{i2c}{3\epsilon}(\xi_2-\xi)^{3/2}} \tilde{\Phi}_{1,\mathrm{reg}}(\xi), \tag{B5}$$

where

$$a_1' = a_1 e^{\frac{i}{\epsilon}\int_{\xi_1}^{\xi_2} k_1(\xi)d\xi}. \tag{B6}$$

For $\Psi_2(\xi)$, we have to address the matching problem across ξ_5. Let us write

$$\Psi_2(\xi) = a_2(-k_2'(\xi))^{1/2} e^{\frac{i}{\epsilon}\int_{\xi_1}^{\xi} k_2^<(\xi')d\xi'} e(\xi, k_2^<(\xi)) \tag{B7}$$

if $\xi_1 \leqslant \xi \leqslant \xi_5$, and

$$\Psi_2(\xi) = a_2'(-k_2'(\xi))^{1/2} e^{-\frac{i}{\epsilon}\int_{\xi}^{\xi_2} k_2^>(\xi')d\xi'} e(\xi, k_2^>(\xi)) \tag{B8}$$

if $\xi_5 \leqslant \xi \leqslant \xi_2$. Here $k_2^>(\xi) - k_2^<(\xi) = 2\pi$. This leads to

$$e^{\frac{i}{\epsilon}k_2^>(\xi_5)\xi} = e^{\frac{i}{\epsilon}k_2^<(\xi_5)\xi} \tag{B9}$$

for $\xi = n\epsilon$, n integer. Then, we obtain

$$a_2' = (-1)^w a_2 e^{\frac{i}{\epsilon}(\int_{\xi_1}^{\xi_5} k_2^<(\xi)d\xi + \int_{\xi_5}^{\xi_2} k_2^>(\xi)d\xi + 2\pi\xi_5)}. \tag{B10}$$

Note that ξ_5 is not necessarily an integer multiple of ξ. It is thus important to keep the last term of the exponential factor in Eq. (B10). The winding number w is around the origin of the ellipse described by $\Gamma(k)$ as k increases by 2π. As explained in the main text, $w = 0$ if the origin lies outside the ellipse, and $w = \pm 1$ if it lies inside. From the expression of $e(\xi, k)$ given in Sec. III of the Supplemental Material [44], we get $e(\xi, k + 2\pi) = (-1)^w e(\xi, k)$. With this definition of $\Psi_2(\xi)$, it behaves as follows near ξ_2:

$$\Psi_2(\xi) \simeq \frac{a_2'}{(\xi_2 - \xi)^{1/4}} e^{-\frac{i2c}{3\epsilon}(\xi_2 - \xi)^{3/2}} \tilde{\Phi}_{2,\mathrm{reg}}(\xi). \tag{B11}$$

As for the turning point near ξ_1, $\tilde{\Phi}_{1,\mathrm{reg}}(\xi_2) = \tilde{\Phi}_{2,\mathrm{reg}}(\xi_2)$, so matching with Airy functions leads to

$$a_1' = -ia_2'. \tag{B12}$$

From the matching conditions Eqs. (B4) and (B12), and the propagation rules for the amplitudes [see Eqs. (B6) and (B10)], we obtain the Bohr-Sommerfeld quantization condition:

$$(-1)^w e^{\frac{i}{\epsilon}\left(\int_{\xi_1}^{\xi_5} k_2^<(\xi)d\xi + \int_{\xi_5}^{\xi_2} k_2^>(\xi)d\xi + 2\pi\xi_5 - \int_{\xi_1}^{\xi_2} k_1(\xi)d\xi\right)} = 1. \tag{B13}$$

This can be recast in a much more appealing way, introducing $\langle\xi\rangle_\sigma = \int_{-\pi}^{\pi} \frac{dk}{2\pi} \xi_\sigma(k)$, where $\xi_\sigma(k)$ denotes the piece of the classical trajectory such that $\sigma(E + \xi_\sigma(k)) > 0$, $\sigma = \pm 1$. Then, the quantization condition becomes

$$(-1)^w e^{i\frac{2\pi\langle\xi\rangle_\sigma}{\epsilon}} = 1. \tag{B14}$$

The above discussion has considered $\sigma = -1$, but the $\sigma = 1$ case is completely analogous.

The solution of Eq. (B14) reads

$$\langle\xi\rangle_\sigma = (2n + w)\omega_0, \tag{B15}$$

with n an arbitrary integer. To go further, it is useful to recall Eq. (A11) for the classical trajectories. It can be recast as

$$E + \xi_\sigma(k) = \sigma E_A(k), \tag{B16}$$

where $E_A(k)$ is positive and 2π-periodic in k. Taking averages over k, Eq. (B15) becomes

$$E = \sigma\langle E_A\rangle - (2n + w)\omega_0. \tag{B17}$$

This is the semiclassical form of a single infinite Wannier-Stark ladder, one for each value of σ. Using this expression in (B16), we see that quantization selects an infinite discrete family of classical orbits given by

$$\xi_\sigma(k) = \sigma(E_A(k) - \langle E_A\rangle) + (2n + w)\omega_0. \tag{B18}$$

2. Tunneling processes: $\mathcal{N} = 1$ case

In the time-dependent picture, Landau-Zener tunneling induces transitions between the two Andreev levels at any finite voltage. In the Floquet picture, the effective Hamiltonian becomes time-independent, but with an additional linear potential $-\xi$. In the classically forbidden regions $\xi_2 < \xi < \xi_3$, Landau-Zener transitions are captured by semiclassical solutions associated with complex k-values. As shown in Fig. 4(c), there are two complex k paths connecting the top of the negative energy Andreev subband to the bottom of the positive energy Andreev subband. For each ξ such that $\xi_2 < \xi < \xi_3$, the two values of $k(\xi)$ on these paths are mutually conjugate. Let us denote by $k_\tau(\xi)$ the branch such that the sign of $\mathrm{Im}(k_\tau(\xi))$ is the sign of $\tau = \pm 1$. Then $k_+(\xi) = k_-(\xi)^*$ when $\xi \in [\xi_2, \xi_3]$.

On this interval, it is then natural to write $\Psi(\xi) = \Psi_+(\xi) + \Psi_-(\xi)$, with

$$\Psi_\tau(\xi) = c_\tau(-i\tau k_\tau'(\xi))^{1/2} e^{\frac{i}{\epsilon}\int_{\xi_2}^{\xi} k_\tau(\xi')d\xi'} e(\xi, k_\tau(\xi)). \tag{B19}$$

Note that $\Psi_+(\xi)$ is a semiclassical solution that decreases as ξ moves away from ξ_2, and which therefore increases as ξ moves away from ξ_3.

However, a closer inspection reveals that this form is not correctly written because one of the components of the local frame $e(\xi, k_\tau(\xi))$ diverges as $\xi + E \to 0$. Indeed, if $E + \xi = 0$, we have $\rho(k_+)\rho(k_-) = 0$, with $\rho(k) = |\Gamma(k)|$. Let us denote by $\tilde{\tau}$ the value of τ such that $\rho(k_{\tilde{\tau}}) = 0$ as $E + \xi = 0$. From the expressions given in Sec. III of the Supplemental Material [44] for the local frame $e(\xi, k_\tau(\xi))$, we see that, if the definition (B19) holds when $\xi_2 < \xi < -E$, then the smooth solution matching this one at $E + \xi = 0$ becomes, when $-E < \xi < \xi_3$,

$$\Psi_\tau(\xi) = \tilde{\tau}\tau c_\tau(i\tau k_\tau'(\xi))^{1/2} e^{\frac{i}{\epsilon}\int_{\xi_2}^{\xi} k_\tau(\xi')d\xi'} e(\xi, k_\tau(\xi)). \tag{B20}$$

From Eqs. (B19) and (B20), we deduce that the connection on the bundle $\mathcal{B}$ has a nontrivial holonomy along the closed path defined by the composition of the two branches $\xi \to k_\tau(\xi)$, oriented in such a way that ξ increases from ξ_2 to ξ_3 (ξ decreases from ξ_3 to ξ_2) when $\tau = 1$ ($\tau = -1$). This is a consequence of the presence of an extra global τ factor in Eq. (B20), which is absent in Eq. (B19). Taking this relative sign into account, we can write down the Airy matching conditions on both sides of ξ_2 as

$$\frac{c_-}{c_+} = (2i)\frac{1 - (-1)^w e^{i\frac{2\pi\langle\xi\rangle_-}{\epsilon}}}{1 + (-1)^w e^{i\frac{2\pi\langle\xi\rangle_-}{\epsilon}}}. \tag{B21}$$

Likewise, across ξ_3, we get

$$\frac{d_+}{d_-} = (2i)\frac{1 - (-1)^w e^{i\frac{2\pi\langle\xi\rangle_+}{\epsilon}}}{1 + (-1)^w e^{i\frac{2\pi\langle\xi\rangle_+}{\epsilon}}}, \tag{B22}$$

with $d_\pm = \exp\left(\frac{i}{\epsilon}\int_{\xi_2}^{\xi_3} k_\pm(\xi)d\xi\right)c_\pm$. It is convenient to write $d_+ = \lambda c_+$ and $d_- = (\lambda^*)^{-1}c_-$ with $|\lambda| < 1$. The Bohr-Sommerfeld condition takes the form

$$\frac{1 - (-1)^w e^{i\frac{2\pi\langle\xi\rangle_-}{\epsilon}}}{1 + (-1)^w e^{i\frac{2\pi\langle\xi\rangle_-}{\epsilon}}} \frac{1 - (-1)^w e^{i\frac{2\pi\langle\xi\rangle_+}{\epsilon}}}{1 + (-1)^w e^{i\frac{2\pi\langle\xi\rangle_+}{\epsilon}}} = -\frac{|\lambda|^2}{4}, \tag{B23}$$

where λ is the strength of the tunneling amplitude associated with Landau-Zener-Stückelberg processes. The previous version of the Bohr-Sommerfeld condition [see Eq. (B17) above and Eq. (39) in the main text] is recovered in the limit of vanishingly small $|\lambda|$.

Now, tunneling is treated as a small perturbation. We have to distinguish between the cases of equal or unequal values of $\exp(2i\pi\langle\xi\rangle_+/\epsilon)$ and $\exp(2i\pi\langle\xi\rangle_-/\epsilon)$. For equal values, we find

$$\delta E_\sigma = i\frac{\epsilon\lambda^2}{4\pi}\frac{1 + (-1)^w e^{i\frac{2\pi\langle\xi\rangle_{-\sigma}}{\epsilon}}}{1 - (-1)^w e^{i\frac{2\pi\langle\xi\rangle_{-\sigma}}{\epsilon}}}, \tag{B24}$$

where δE_σ is real-valued. The wave function is mostly localized on the σ piece of the classical trajectory.

The situation changes qualitatively in the degenerate case. The degeneracy is lifted at first order in $|\lambda|$ according to

$$\delta E_\sigma = \pm\sigma \frac{\epsilon}{2\pi}|\lambda|. \tag{B25}$$

The right-hand side of Eq. (B25) is much larger than its counterpart in Eq. (B24) at small $|\lambda|$. This is the analog of energy level repulsion in the setting of Floquet theory for time-periodic Hamiltonians. This phenomenon has already been reported in our previous numerical study [33].

The support of the semiclassical wave function is very different, depending on whether the uncoupled Wannier-Stark ladders are distinct or degenerate. In the nondegenerate case, the solutions are strongly localized on one piece σ of the classical trajectory. In the degenerate case, they are linear superpositions with equal weights of semiclassical wave functions associated with *both* pieces of the classical trajectory. These superpositions appear clearly in the resolvent when the two Wannier-Stark ladders are nearly degenerate, as shown in Fig. 2 of the Supplemental Material [44].

3. Tunneling processes: $\mathcal{N} = 2$ case

Let us now consider the case when the function $\xi(k)$ on either piece of the classical trajectory has two minima and two maxima when k increases from $-\pi$ to π, i.e., $\mathcal{N} = 2$. As shown in Fig. 4(a), the two classically allowed regions are now connected by two tunneling loops. More of the notations used here are shown in Fig. 7. Imposing the Airy matching rules at each of the two turning points located at the extremities of the tunneling loop gives

$$\begin{pmatrix} a'_2 \\ b'_2 \end{pmatrix} = S_1 \begin{pmatrix} a'_1 \\ b'_1 \end{pmatrix}, \quad \begin{pmatrix} a'_4 \\ b'_4 \end{pmatrix} = S_2 \begin{pmatrix} a'_3 \\ b'_3 \end{pmatrix}, \tag{B26}$$

with

$$S_j = i \begin{pmatrix} (1-\eta_j^2)^{1/2} & \eta_j e^{-i\theta_j} \\ \eta_j e^{i\theta_j} & -(1-\eta_j^2)^{1/2} \end{pmatrix}. \tag{B27}$$

Denoting by $k_{j,+}(\xi)$ the tunneling branch with a positive imaginary part for k, we set $\lambda_j = \exp\left(\frac{i}{\epsilon}\int k_{j,+}(\xi)\, d\xi\right)$, where the integral is taken on the jth tunneling path ($j = 1, 2$), and $|\lambda_j| \ll 1$ in the small voltage limit. Then, the parameters entering the unitary matrix S_j are

$$\eta_j = \frac{|\lambda_j|}{1 + \frac{|\lambda_j|^2}{4}}, \quad e^{i\theta_j} = \tilde{\tau}_j \frac{\lambda_j}{|\lambda_j|}, \tag{B28}$$

where $\tilde{\tau}_j = \pm 1$. Between the two tunneling loops, we have the usual semiclassical propagation of amplitudes:

$$\begin{pmatrix} a'_3 \\ b'_3 \end{pmatrix} = P_1 \begin{pmatrix} a'_2 \\ b'_2 \end{pmatrix}, \quad \begin{pmatrix} a'_4 \\ b'_4 \end{pmatrix} = P_2 \begin{pmatrix} a'_3 \\ b'_3 \end{pmatrix}, \tag{B29}$$

with

$$P_j = -i \begin{pmatrix} e^{i\varphi_{jL}} & 0 \\ 0 & -e^{i\varphi_{jR}} \end{pmatrix}. \tag{B30}$$

The phase factors $e^{i\varphi_{jL}}$ and $e^{i\varphi_{jR}}$ are expressed in terms of oscillating integrals of the form $\exp\left(\frac{i}{\epsilon}\int k(\xi)\, d\xi\right)$ taken on appropriate paths. When $j = 2$, an extra Berry phase factor $(-1)^w$ has to be taken into account. Setting $M = P_2 S_2 P_1 S_1$, the Bohr-Sommerfeld quantization condition reads

$$\det(M - I) = 0. \tag{B31}$$

The entries of M are

$$M_{11} = \left(1-\eta_1^2\right)^{1/2}\left(1-\eta_2^2\right)^{1/2} e^{i\varphi_L} - \eta_1\eta_2 e^{i(\varphi_{1R}+\varphi_{2L}+\theta_1-\theta_2)},$$

$$M_{22} = \left(1-\eta_1^2\right)^{1/2}\left(1-\eta_2^2\right)^{1/2} e^{i\varphi_R} - \eta_1\eta_2 e^{i(\varphi_{1L}+\varphi_{2R}-\theta_1+\theta_2)},$$

$$M_{12} = \eta_1\left(1-\eta_2^2\right)^{1/2} e^{i(\varphi_L-\theta_1)} + \eta_2\left(1-\eta_1^2\right)^{1/2} e^{i(\varphi_{1R}+\varphi_{2L}-\theta_2)},$$

$$-M_{21} = \eta_1\left(1-\eta_2^2\right)^{1/2} e^{i(\varphi_L+\theta_1)} + \eta_2\left(1-\eta_1^2\right)^{1/2} e^{i(\varphi_{1L}+\varphi_{2R}+\theta_2)}.$$

Here, we have introduced $\varphi_L = \varphi_{1L} + \varphi_{2L}$, $\varphi_R = \varphi_{1R} + \varphi_{2R}$. If we shift the energy E by δE, Eq. (A11) shows that the classical trajectory is shifted along the ξ axis by $\delta\xi = -\delta E$. A simple analysis (using integration by parts) of the phase factors involved in the entries of M shows that M is multiplied by $\exp(i\frac{2\pi\delta E}{\epsilon})$. This implies that the Bohr-Sommerfeld quantization condition is invariant when E is shifted by integer multiples of $\epsilon = 2eV/\hbar$, and therefore we get a periodic Wannier-Stark ladder spectrum.

Let us now treat tunnel amplitudes η_1, η_2 as small perturbations. When these amplitudes vanish (e.g., as the bias voltage $V \to 0$), Eq. (B31) becomes $(e^{i\varphi_L} - 1)(e^{i\varphi_R} - 1) = 0$, and we have two uncoupled ladders, one associated with each piece of the classical trajectory. When we switch on small tunneling amplitudes, we have to distinguish between the nondegenerate case $e^{i\varphi_L} \neq e^{i\varphi_R}$ and the degenerate one. In the former case, the energy shift δE for the left ladder (we assume $e^{i\varphi_L} = 1$) is

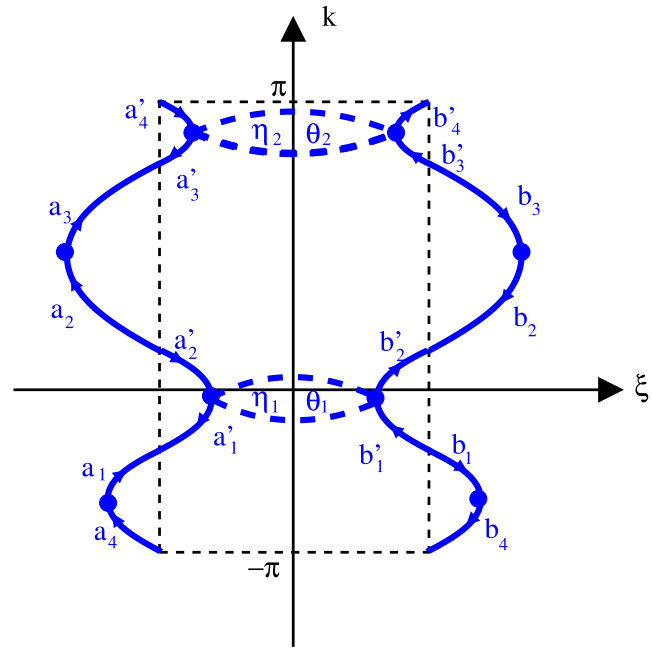

FIG. 7. Semiclassical wave function for $\mathcal{N} = 2$: The semiclassical trajectory $\mathcal{T}_{E,-}$ ($\mathcal{T}_{E,+}$) exhibits now four turning points. Classical trajectories $\mathcal{T}_{E,-}$ and $\mathcal{T}_{E,+}$ are depicted by full lines, and they are connected by a pair of tunneling loops depicted by dashed lines. These tunneling loops are characterized by tunneling amplitudes η_1, η_2 and by tunneling phases θ_1, θ_2. Arrows near turning points indicate an increasing phase function $\theta(\xi)$ along classical trajectories.

given by

$$\frac{2\pi\delta E}{\epsilon} = \frac{\eta_1^2+\eta_2^2}{2}\cot\left(\frac{\varphi_R}{2}\right) + \eta_1\eta_2\frac{\cos(\varphi_{1L}+\frac{\varphi_{2R}-\varphi_{1R}}{2}-\theta_1+\theta_2)}{\sin(\frac{\varphi_R}{2})}. \tag{B32}$$

The energy shift for the right ladder is given by a similar expression, after replacing R by L. In the degenerate case ($e^{i\varphi_L} = e^{i\varphi_R} = 1$), the degenerate levels are repelled from each other according to

$$\frac{2\pi\delta E}{\epsilon} = \pm\left[\eta_1^2+\eta_2^2+2\eta_1\eta_2\cos(\varphi_{1L}+\varphi_{2R}-\theta_1+\theta_2)\right]^{1/2}. \tag{B33}$$

Here, the new qualitative feature is the presence of interferences between the two tunneling paths. They appear via the voltage-dependent phases θ_1 and θ_2 in Eqs. (B33) and (B33). For an illustration of such interferences, see Fig. 4(d) in Ref. [34].

[1] M. Berry, The geometric phase, Sci. Am. **259**, 46 (1988).

[2] S. Pancharatnam, Generalized theory of interference, and its applications, Proc. Ind. Acad. Sci. A **44**, 247 (1956).

[3] H. C. Longuet-Higgins, U. Öpik, M. H. L. Pryce, and R. A. Sack, Studies of the Jahn-Teller effect. II. The dynamical problem, Proc. R. Soc. A **244**, 1 (1958).

[4] M. V. Berry, Quantal phase factors accompanying adiabatic changes, Proc. R. Soc. London A **392**, 45 (1984).

[5] A. Bohm, A. Mostafazadeh, H. Koizumi, Q. Niu, and J. Zwanziger, *The Geometric Phase in Quantum Systems: Foundations, Mathematical Concepts, and Applications in Molecular and Condensed Matter Physics* (Springer-Verlag, Berlin, 2003).

[6] D. Xiao, M.-C. Chang, and Q. Niu, Berry phase effects on electronic properties, Rev. Mod. Phys. **82**, 1959 (2010).

[7] G. Falci, R. Fazio, G. M. Palma, J. Siewert, and V. Vedral, Detection of geometric phases in superconducting nanocircuits, Nature (London) **407**, 355 (2000).

[8] Y. Makhlin, G. Schön, and A. Shnirman, Quantum-state engineering with Josephson-junction devices, Rev. Mod. Phys. **73**, 357 (2001).

[9] P. J. Leek, J. M. Fink, A. Blais, R. Bianchetti, M. Göppl, J. M. Gambetta, D. I. Schuster, L. Frunzio, R. J. Schoelkopf, and A. Wallraff, Observation of Berry's phase in a solid state qubit, Science **318**, 1889 (2007).

[10] J. A. Jones, V. Vedral, A. Ekert, and G. Castagnoli, Geometric quantum computation using nuclear magnetic resonance, Nature (London) **403**, 869 (2000).

[11] M. Z. Hasan and C. L. Kane, Colloquium: Topological insulators, Rev. Mod. Phys. **82**, 3045 (2010).

[12] A. Fert, N. Reyren, and V. Cros, Magnetic skyrmions: advances in physics and potential applications, Nat. Rev. Mater. **2**, 17031 (2017).

[13] A. V. Shytov, M. S. Rudner, and L. S. Levitov, Klein Backscattering and Fabry-Pérot Interference in Graphene Heterojunctions, Phys. Rev. Lett. **101**, 156804 (2008).

[14] A. F. Young and P. Kim, Quantum interference and Klein tunneling in graphene heterojunctions, Nat. Phys. **5**, 222 (2009).

[15] A. Varlet, M.-H. Liu, V. Krueckl, D. Bischoff, P. Simonet, K. Watanabe, T. Taniguchi, K. Richter, K. Ensslin, and T. Ihn, Fabry-Pérot Interference in Gapped Bilayer Graphene with Broken Anti-Klein Tunneling, Phys. Rev. Lett. **113**, 116601 (2014).

[16] R. Du, M.-H. Liu, J. Mohrmann, F. Wu, R. Krupke, H. von Löhneysen, K. Richter, and R. Danneau, Tuning Anti-Klein to Klein Tunneling in Bilayer Graphene, Phys. Rev. Lett. **121**, 127706 (2018).

[17] R. Resta, Manifestations of Berry's phase in molecules and condensed matter, J. Phys.: Condens. Matter **12**, R107 (2000).

[18] W. Yao and Q. Niu, Berry Phase Effect on the Exciton Transport and on the Exciton Bose-Einstein Condensate, Phys. Rev. Lett. **101**, 106401 (2008).

[19] T. Gao, E. Estrecho, K. Y. Bliokh, T. C. H. Liew, M. D. Fraser, S. Brodbeck, M. Kamp, C. Schneider, S. Höfling, Y. Yamamoto, F. Nori, Y. S. Kivshar, A. G. Truscott, R. G. Dall, and E. A. Ostrovskaya, Observation of non-Hermitian degeneracies in a chaotic exciton-polariton billiard, Nature (London) **526**, 554 (2015).

[20] D. M. Badiane, M. Houzet, and J. S. Meyer, Nonequilibrium Josephson Effect Through Helical Edge States, Phys. Rev. Lett. **107**, 177002 (2011).

[21] M. Houzet, J. S. Meyer, D. M. Badiane, and L. I. Glazman, Dynamics of Majorana States in a Topological Josephson Junction, Phys. Rev. Lett. **111**, 046401 (2013).

[22] D. M. Badiane, L. I. Glazman, M. Houzet, and J. S. Meyer, ac Josephson effect in topological Josephson junctions, C. R. Phys. **14**, 840 (2013).

[23] B. van Heck, S. Mi, and A. R. Akhmerov, Single fermion manipulation via superconducting phase differences in multiterminal Josephson junctions, Phys. Rev. B **90**, 155450 (2014).

[24] C. Padurariu, T. Jonckheere, J. Rech, R. Mélin, D. Feinberg, T. Martin, and Yu. V. Nazarov, Closing the proximity gap in a metallic Josephson junction between three superconductors, Phys. Rev. B **92**, 205409 (2015).

[25] R.-P. Riwar, M. Houzet, J. S. Meyer, and Y. V. Nazarov, Multiterminal Josephson junctions as topological materials, Nat. Commun. **7**, 11167 (2016).

[26] E. Strambini, S. D'Ambrosio, F. Vischi, F. S. Bergeret, Yu. V. Nazarov, and F. Giazotto, The ω-SQUIPT as a tool to phase-engineer Josephson topological materials, Nat. Nanotechnol. **11**, 1055 (2016).

[27] E. Eriksson, R.-P. Riwar, M. Houzet, J. S. Meyer, and Y. V. Nazarov, Topological transconductance quantization in a four-terminal Josephson junction, Phys. Rev. B **95**, 075417 (2017).

[28] A. Freyn, B. Douçot, D. Feinberg and R. Mélin, Production of Non-Local Quartets and Phase-Sensitive Entanglement in a Superconducting Beam Splitter, Phys. Rev. Lett. **106**, 257005 (2011).

[29] T. Jonckheere, J. Rech, T. Martin, B. Douçot, D. Feinberg, and R. Mélin, Multipair dc Josephson resonances in a biased all-superconducting bijunction, Phys. Rev. B **87**, 214501 (2013).

[30] A. H. Pfeffer, J. E. Duvauchelle, H. Courtois, R. Mélin, D. Feinberg, and F. Lefloch, Subgap structure in the conductance

of a three-terminal Josephson junction, Phys. Rev. B **90**, 075401 (2014).

[31] R. Mélin, D. Feinberg, and B. Douçot, Partially resummed perturbation theory for multiple Andreev reflections in a short three-terminal Josephson junction, Eur. Phys. J. B **89**, 67 (2016).

[32] Y. Cohen, Y. Ronen, J. H. Kang, M. Heiblum, D. Feinberg, R. Mélin, and H. Strikman, Non-local supercurrent of quartets in a three-terminal Josephson junction, Proc. Natl. Acad. Sci. USA **115**, 6991 (2018).

[33] R. Mélin, J.-G. Caputo, K. Yang, and B. Douçot, Simple Floquet-Wannier-Stark-Andreev viewpoint and emergence of low-energy scales in a voltage-biased three-terminal Josephson junction, Phys. Rev. B **95**, 085415 (2017).

[34] R. Mélin, R. Danneau, K. Yang, J.-G. Caputo, and B. Douçot, Engineering the Floquet spectrum in superconducting multiterminal quantum dots, Phys. Rev. B **100**, 035450 (2019).

[35] S. N. Shevchenko, S. Ashhab, and F. Nori, Landau-Zener-Stückelberg interferometry, Phys. Rep. **492**, 1 (2010).

[36] E. Dupont-Ferrier, B. Roche, B. Voisin, X. Jehl, R. Wacquez, M. Vinet, M. Sanquer, and S. De Franceschi, Coherent Coupling of Two Dopants in a Silicon Nanowire Probed by Landau-Zener-Stückelberg Interferometry.Phys. Rev. Lett. **110**, 136802 (2013).

[37] G. H. Wannier, Wave-Functions and Effective Hamiltonian for Bloch Electrons in an Electric Field, Phys. Rev. **117**, 432 (1960).

[38] F. Bentosela, V. Grecchi, and F. Zironi, Oscillations of Wannier Resonances, Phys. Rev. Lett. **50**, 84 (1983).

[39] V. Guillemin and S. Sternberg, *Geometric Asymptotics*, Mathematical Surveys and Monographs Vol. 14 (American Mathematical Society, Somerville, Massachusetts, 1977); see, in particular, Chap. II.

[40] M. Wilkinson, An example of phase holonomy in WKB theory, J. Phys. A **17**, 3459 (1984).

[41] Y. Y. Wang, B. Pannetier, and R. Rammal, Quasiclassical approximations for almost-Mathieu equations, J. Phys. (France) **48**, 2067 (1987).

[42] L. D. Landau and E. M. Lifshitz, *Quantum Mechanics*, 3rd ed. (Butterworth-Heinemann, Oxford, 2008).

[43] E. N. Bratus', V. S. Shumeiko, E. V. Bezuglyi, and G. Wendin, dc-current transport and ac Josephson effect in quantum junctions at low voltage, Phys. Rev. B **55**, 12666 (1997).

[44] See Supplemental Material at http://link.aps.org/supplemental/10.1103/PhysRevB.101.035411 for technical details of the analytical calculations.